American Mineralogist, Volume 77, pages 507–511, 1992

Crystal structure refinement of a spinelloid in the system Fe_3O_4-Fe_2SiO_4

C. R. Ross II
Bayerisches Geoinstitut, Universität Bayreuth, Postfach 10 12 51, W-8580 Bayreuth, Germany
T. Armbruster
Laboratorium für chemische und mineralogische Kristallographie, Universität Bern, Freiestrasse 3, CH-3012 Bern, Switzerland
D. Canil
Bayerisches Geoinstitut, Universität Bayreuth, Postfach 10 12 51, W-8580 Bayreuth, Germany

Abstract

A spinelloid phase has been synthesized at 1200 °C, 7 GPa from the approximate composition $Fe_{5.2}Si_{0.8}O_8$ (Fa_{40}-Mt_{60}). X-ray precession photographs indicated that it is probably isostructural with nickel aluminosilicate V. The photographs and backscattered electron imaging, however, also indicate the presence of at least one other phase, of lower Fe content, as oriented lamellar inclusions in the spinelloid phase. Single crystal data were measured, and the structure was refined in space group *Pmma* [a = 5.867(1) Å, b = 8.917(1) Å, c = 8.362(1) Å] to an R factor of 4.24%, confirming that this phase is isostructural with nickel aluminosilicate V. Refinement of tetrahedral site occupancies leads to a bulk composition of $Fe_{5.36}Si_{0.64}O_8$ ($Fa_{32}Mt_{68}$), which is corroborated by bond-length analysis of the refined structure.

Introduction

Phase equilibrium experiments at high pressures in peridotitic systems have shown that silicate spinels and spinelloids may be important phases in a peridotitic upper mantle at depths between 400 and 650 km (e.g., Takahashi and Ito, 1987). For the composition Mg_2SiO_4, the stable phase at low pressure is forsterite, with the olivine (or α-Mg_2SiO_4) structure. With increasing pressure, α-Mg_2SiO_4 converts to the β-Mg_2SiO_4 structure and to the spinel (γ-Mg_2SiO_4) structure (Ringwood and Major, 1970). The β-Mg_2SiO_4 structure is related to the spinel phase in that discrete structural layers in the β phase are topologically equivalent to layers found in the spinel structure; the two structures differ primarily in the stacking of these layers and thus can be considered as stacking polytypes and members of a more general group of materials, the spinelloids.

Spinelloid polytypes have been observed in a variety of systems, including $NiAl_2O_4$-Ni_2SiO_4 (Ma, 1974; Ma et al., 1975; Ma and Tillmans, 1975; Ma and Sahl, 1975; Horioka et al., 1981a, 1981b), $MgGa_2O_4$-Mg_2GeO_4 and $MgFe_2O_4$-Mg_2GeO_4 (Barbier, 1989), $NiGa_2O_4$-Ni_2SiO_4 (Hammond and Barbier, 1991), Co_2SiO_4 (Akimoto and Sato, 1968), and Mg_2SiO_4 (Ringwood and Major, 1970). Both qualitative and semiquantitative models have been devised to relate the occurrence of the spinelloid phases with variation in temperature and pressure of formation (Hazen and Finger, 1981; Price, 1983; Price et al., 1985).

Recently, high-pressure phase equilibrium experiments have revealed the presence of a spinelloid phase for intermediate compositions in the Fe_3O_4-Fe_2SiO_4 system (Canil et al., 1990). In this paper, we report on a single-crystal structure analysis of this spinelloid phase. Complete high-pressure phase relations along the Fe_3O_4-Fe_2SiO_4 join will be reported elsewhere. The discovery and description of spinelloid structures in this system may be important for understanding the crystal chemistry of spinelloids in general and may also be relevant to the crystal chemistry of Fe^{3+} and Fe^{2+} in the transition region of the Earth's upper mantle.

Experimental procedures

Starting materials for experiments along the join Fe_3O_4-Fe_2SiO_4 were mixtures of reagent grade Fe_3O_4 (Johnson Matthey, 99.5% purity) and pure fayalite (synthesized at 1 atm from reagent grade Fe_2O_3 and SiO_2). These mixtures were loaded in 2.2-mm diameter Au capsules and sealed by arc welding. Experiments were performed at 7 GPa and 950–1200 °C in a Sumitomo 1200 split-sphere multianvil apparatus using Toshiba F grade WC cubes having an 11-mm truncated edge length for pressure generation, and 18-mm edged Cr_2O_3-doped MgO octahedra as pressure media. Temperature was measured with a Pt-$Pt_{87}Rh_{13}$ thermocouple isolated from the capsule by a disk of MgO. The temperature was not corrected for the pressure effect on thermocouple emf. Durations of experiments ranged from 15 h at 950 °C to 5 h at 1200 °C. Details of the furnace assembly and pressure calibration employed in these experiments are given elsewhere (Canil, 1991).

The product of a preliminary experiment at 7 GPa and 1200 °C on material of bulk composition $Fa_{40}Mt_{60}$ was found by powder X-ray diffraction analysis to consist

0003–004X/92/0506–0507$02.00

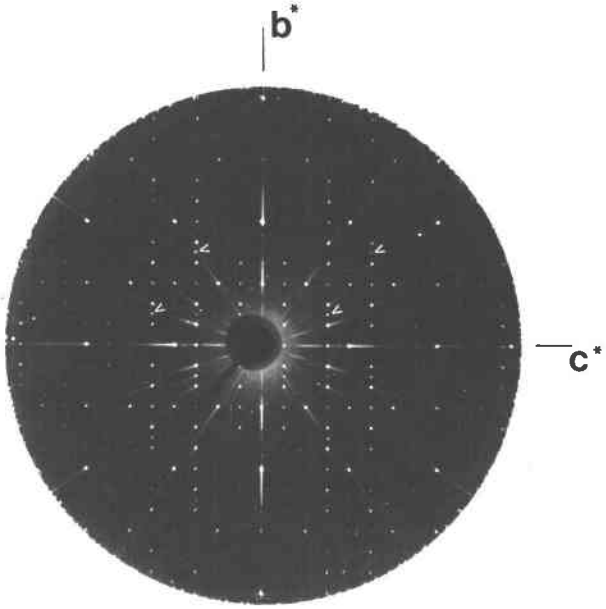

Fig. 1. Precession photograph of the $0kl$ reciprocal lattice plane of the major phase. Some reflections of the minor phase are marked: note difference in lattice symmetry ($2mm$ vs. 2) in this section.

(within the limits of resolution) entirely of a phase that was not spinel. A second synthesis was then performed under identical conditions with the goal of recovering single crystals for structure analysis.

Several single crystals up to 500 μm in size were extracted from these latter synthesis products. The remaining material was mounted for electron microprobe analysis. The crystals are black and ferromagnetic.

Electron microprobe analysis

Polished sections of the latter synthesis product were examined by electron microprobe analysis (EMPA) using a Cameca SX50 instrument in wavelength dispersive mode. Operating conditions were 15 kV, probe current of 12 nA, and counting times of 20 s on peaks. Hematite (Fe) and orthoclase (Si) were used as standards.

The material separated for electron microprobe analysis was examined by backscattered electron imaging. These images showed that the crystals consist of a groundmass (the "major phase" hereafter) with included lamellae ca. 0.5 μm in width and apparently 2–5 μm long, which make up an estimated 10–20% (by volume) of the material. These lamellae (the "minor phase" hereafter) appear to bear a fixed orientation to the major phase, and on the basis of backscattered electron intensity appear to have a slightly lower average atomic number than the major phase; this could be interpreted to indicate that the minor phase is slightly Fe depleted relative to the major phase. Unfortunately, the lamellae were too small to analyze by EMPA; therefore the compositional difference remains inferential. Although some Bragg reflections from the minor phase could be identified on precession photographs (see below), the orientational relationship between the two phases could not be conclusively determined.

Crystallography

Several of the crystals separated for structure analysis were examined with a precession camera. Of these, one was chosen for detailed study, and several diffraction patterns were obtained. The photographs revealed the presence of at least two distinct phases, identified with the major and minor phases found by EMPA on the basis of the relative intensity of reflections belonging to each.

The space group of the major phase was found to be *Pmma*. Despite considerable efforts, reflections corresponding to the minor phase were only found in one photograph (Fig. 1), corresponding to the $0kl$ reciprocal lattice plane of the major phase. The reflections from the minor phase are distinguishable from those of the major phase by a difference of plane symmetry in this photograph; the minor-phase reflections show only the required inversion symmetry, whereas the major-phase reflections show $2mm$ symmetry. Further details of the minor phase are discussed below.

Using the constraints of space group, unit-cell dimensions, and bulk composition of the major phase, the Inorganic Crystallographic Structure Database (Bergerhoff et al., 1983) was examined for possible structures; a candidate structure was found in the nickel aluminosilicate V structure of Horioka et al. (1981b).

In the absence of single-phase crystals, intensity data were measured using a four-circle diffractometer. A second crystal with dimensions 0.20 × 0.15 × 0.12 mm was selected and mounted on an Enraf-Nonius CAD4 diffractometer. After preliminary inspection of the crystal to ascertain its quality, 23 reflections with θ between 18 and 22° were centered and the unit-cell dimensions refined (Table 1). The differences between cell dimensions measured from precession photographs and those refined from centering of reflections are probably insignificant, considering the differences in the methods and the problems with overlapped peaks.

A set of 3028 reflections was measured at room temperature in ω-θ mode to approximately $\sin(\theta)/\lambda = 0.9$ using graphite-monochromated Mo$K\alpha$ radiation (λ = 0.71069 Å). The orientation of the crystal was checked after every 100 measured reflections, and the intensity of representative reflections was checked every 3 h. To assess the problem of interference from the minor phase, all reflections of indices $10 > h \geq 0$, $15 > k \geq 0$, and $15 > l > -15$ were measured; this yielded two symmetrically equivalent reflections for reflections with $l \neq 0$. Equivalent reflections were averaged, yielding 1588 independent reflections; the agreement factor for averaging was 2.1% (on I). After rejection of systematically absent reflections (none of which had observable intensity), careful scrutiny for interference from the minor phase (by comparison of the intensities of reflections hkl and $hk\bar{l}$,

TABLE 1. Final unit-cell dimensions, atomic positional parameters, thermal factors, and site occupancies

Unit cell:		*a*	*b*	*c*	*V*
Film		5.870(1)	8.920(2)	8.366(3)	438.0(2)
Four-circle		5.867(1)	8.917(1)	8.362(1)	437.2(1)
Site	*x*	*y*	*z*	$U_{iso} \times 10^4$	X_{Fe}
M1	¾	0.1659(1)	0.2495(1)	47(2)	1
M2	½	0	0	62(2)	1
M3	½	0.3333(1)	½	52(2)	1
M4	¾	½	0.2185(2)	38(2)	1
T1	¼	0	0.3764(2)	50*	0.84(1)
T2	¼	0.3255(1)	0.1321(2)	50*	0.60(1)
O1	0.5046(13)	0	0.2477(8)	113(11)	—
O2	¼	0.1715(8)	0.0031(7)	110(9)	—
O3	¼	0.1694(8)	0.5010(6)	92(9)	—
O4	0.4951(8)	0.3287(6)	0.2513(6)	109(7)	—
O5	¼	½	0.0280(12)	134(14)	—
O6	¼	½	0.5250(9)	71(11)	—

* U_{iso} constrained to 50×10^{-4} for the tetrahedral sites.

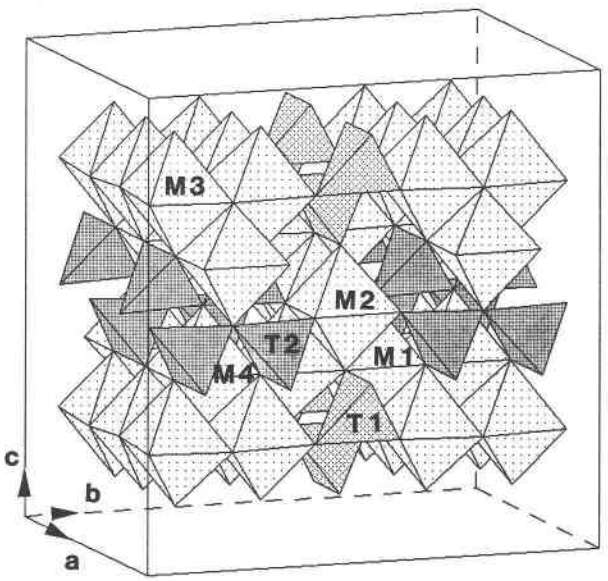

Fig. 2. Perspective polyhedral diagram of the refined $Fa_{40}Mt_{60}$ spinelloid structure. Note that the spinelloid stacking direction is parallel to the **b** axis, i.e., the spinel-like planes are parallel to (010).

which resulted in rejection of all reflections of the form $0kl$), as well as the rejection of the reflection 400 (which suffered from extinction), 1315 reflections remained. Of these, 947 had $F_{obs} > 6\sigma$ and were used in the refinement. An empirical absorption correction based on ψ scans was applied to all reflections.

CRYSTAL STRUCTURE ANALYSIS

The diffractometer data set corroborated the space-group and unit-cell determinations from the precession camera analysis. Refinement of the data using the starting parameters for the nickel aluminosilicate V structure was performed. It was assumed that octahedral sites were occupied by Fe only. As stoichiometry requires that some Fe occupies the tetrahedral sites, these occupancies were refined. High correlations between the site occupancies and thermal parameters, however, required the fixing of $U_{iso} = 50 \times 10^{-4}$ for these sites. A total of 31 parameters were refined using unit weighting. Full matrix least-squares refinement of the structure yielded (in the final cycle) an R factor of 4.24%. The final positional, occupancy, and thermal parameters for this structure are given in Table 1, and the final observed and calculated structure factors are listed in Table 2.[1]

DISCUSSION

Despite problems with interference with the minor phase, the structure refinement is satisfactory, and the identification of the structure of the major phase with that of the nickel aluminosilicate V structure is confirmed. This structure contains six crystallographically distinct cation sites, four of them (M) octahedral and two (T) tetrahedral (Fig. 2). The M1 and M4 sites form infinite edge-sharing strips one octahedron wide along **b**. These strips are crosslinked along **a** by corner sharing with T1 monomers and T2 dimers; edge sharing with M2 and M3 sites establishes connections along **c**. The M2 polyhedron forms an infinite edge-shared strip one octahedron wide along **a**; these strips are linked along **b** by corner sharing of T2 dimers, and by shared edges with the M1 site. Lastly, the M3 polyhedra form an edge-shared strip two octahedra wide running along **a**, crosslinked by the T1 sites and sharing further edges with the M1 and M4 polyhedra. The bond lengths and measures of polyhedral distortion for all sites are given in Table 3.

The tetrahedral bond lengths are significantly longer than the value 1.624 Å predicted for Si-O by the bond-

TABLE 3. Bond lengths and polyhedral distortion indices*

Site	X-O bond length	Quadratic elongation	Angle variance
M1	2× 2.064 Å	1.00037	0.97
	2× 2.084 Å		
	2.084 Å		
	2.113 Å		
M2	2× 2.071 Å	1.00086	2.27
	4× 2.119 Å		
M3	2× 2.071 Å	1.00197	6.88
	2× 2.080 Å		
	2× 2.099 Å		
M4	2.061 Å	1.01149	39.70
	2.145 Å		
	4× 2.155 Å		
T1	2× 1.835 Å	1.00013	0.78
	2× 1.841 Å		
T2	1.746 Å	1.00261	10.81
	2× 1.750 Å		
	1.783 Å		

* Quadratic elongation and angle variance after Hazen and Finger (1982).

[1] A copy of Table 2 may be ordered as Document AM-92-495 from the Business Office, Mineralogical Society of America, 1130 Seventeenth Street NW, Suite 330, Washington, DC 20036, U.S.A. Please remit $5.00 in advance for the microfiche.

TABLE 4. Site occupancy calculation

Ideal bond lengths*	Site	$X_{Fe^{3+}}$
$^{[6]}Fe^{2+}$—2.140 Å	M1	0.462
$^{[6]}Fe^{3+}$—2.016 Å	M2	0.304
$^{[4]}Fe^{3+}$—1.865 Å	M3	0.462
$^{[4]}Si^{4+}$—1.624 Å	M4	0.024
	T1	0.888
	T2	0.552

* Ideal bond lengths based on Brown and Altermatt (1985).

length bond-strength model of Brown and Altermatt (1985), indicating that significant Fe is incorporated in these sites. If we assume that Fe^{2+} is confined to the octahedral sites, and Si to the tetrahedral sites, the ideal bond lengths (Brown and Altermatt, 1985) given in Table 4 yield the site compositions given in that table. Fe^{3+} appears from these calculations to be largely excluded from the M4 site, perhaps because of the strong distortion of this site, whereas the Fe^{3+} contents of the other octahedral sites indicate relatively minor site preference. Both tetrahedral sites show significant amounts of Fe^{3+}; however preference is indicated for the less-distorted T1 site. It should be noted that the tetrahedral site occupancies arrived at in this calculation are in relatively good agreement with those obtained from the structure refinement. These site occupancies yield a bulk composition of $Fe_{5.33}Si_{0.67}O_8$, corresponding to $Fa_{0.34}Mt_{0.66}$. Although this figure is subject to significant error, it indicates a composition somewhat more Fe rich than the bulk composition, as was expected from examination of the backscattered electron images. On the basis of this inferred composition and the unit-cell volume (as measured on the diffractometer), the calculated density of this material at 1 atm is 5.064 g/cm³.

The stability of intermediate spinelloids relative to a physical mixture of end-member spinels is thought to be in part due to an increase in configurational entropy caused by cation disorder (Akaogi and Navrotsky, 1984; Barbier and Hyde, 1986; Leinenweber and Navrotsky, 1989; Hammond and Barbier, 1991), e.g., for nickel aluminosilicate V (Horioka et al., 1981a; Akaogi and Navrotsky, 1984), ΔS_{conf} = 2.09 cal/mol·K (four–O atom basis). Fe_2SiO_4 spinel is nearly perfectly normal (Finger et al., 1979); assuming that Fe_3O_4 is perfectly inverse and ignoring the entropy contribution of electron exchange, ΔS_{conf} = 1.80 cal/mol·K for the structure reported here. Nevertheless, ΔS_{conf} for a spinel with the same composition is still larger (2.22 cal/mol·K), but if the enthalpy of formation of a spinelloid of a composition between a normal and inverse spinel increases with the proportion of spinel-type units (as suggested by Akaogi and Navrotsky, 1984), the nickel aluminosilicate V structure would be favored over that of a spinel. The difference in enthalpy between a spinel solid solution and the spinelloid phases may be due to the variability of sites. In the spinel structure, cations of a variety of sizes are forced to mix on two crystallographic sites, thus setting up local strains due to misfit between coordination polyhedra. The nickel aluminosilicate V structure, with a more complex topology, offers a range of cation sites and thus more opportunity for cation redistribution and adjustment of coordination polyhedra. That this effect (discussed by Hazen and Finger, 1981) is contributory to the stability of the spinelloid is seen in the strong site fractionations. If the sole force stabilizing this phase were entropic, one would expect random distribution on all sites.

A problem still remains as to the identity and structure of the minor phase. In the diffraction pattern of Figure 1, it can be seen that one of the principle reciprocal-lattice translations of the minor phase is parallel to **c*** of the major phase, whereas the second translation in the minor phase is subparallel to **b*** of the major phase. Defining (for present purposes only) these translations in the minor phase as **c*** and **b***, respectively, the lattice parameters are b = 5.914(5) Å, c = 8.346(10) Å, and α = 90.27°; if the unit cell of the minor phase (with respect to the present axes) is centered or contains a glide plane parallel to (100) (which cannot be detected in a single photograph) these axial lengths would be incorrect; the true lengths would be a (probably small) multiple of the given values. These dimensions for the minor phase result in the following relationships: $[001]_{maj} = [001]_{min}$, $[010]_{maj} \cong [010]_{min}$, $c_{maj} \cong c_{min}$, and $2 \times b_{maj} \cong 3 \times b_{min}$.

Cone-axis photographs were taken along both the **a*** and **b*** axes (major phase) to find a crystal orientation that would reveal the remaining lattice parameters of the minor phase. These photographs showed the translations corresponding to the major phase, as well as weak rings corresponding to a translation of 32.09 Å (parallel to $\mathbf{a}^*_{maj}$) and approximately 30 Å (parallel to $\mathbf{b}^*_{maj}$); for these, only the odd-order rings were observed. Long-exposure precession photographs were taken to reveal the lattice planes responsible for these rings but could not be interpreted.

It is unclear whether the present material represents an assemblage of intergrown phases at equilibrium at the pressure and temperature of synthesis (i.e., 7 GPa and 1200 °C) or an exsolution texture developed during quench or decompression. The relations between unit-cell parameters described above are suggestive of some structural similarity between the two phases influencing the nucleation and growth of the phases, e.g., epitaxy, topotaxy, or coherent exsolution. Experiments are underway to elucidate these relationships.

REFERENCES CITED

Akaogi, M., and Navrotsky, A. (1984) Calorimetric study of the stability of spinelloids in the system $NiAl_2O_4$-Ni_2SiO_4. Physics and Chemistry of Minerals, 10, 166–172.

Akimoto, S.-I., and Sato, Y. (1968) High-pressure transformation in Co_2SiO_4 olivine and some geophysical implications. Physics of the Earth and Planetary Interiors, 1, 498–505.

Barbier, J. (1989) New spinelloid phases in the $MgGa_2O_4$-Mg_2GeO_4 and $MgFe_2O_4$-Mg_2GeO_4 systems. European Journal of Mineralogy, 1, 39–46.

Barbier, J., and Hyde, B.G. (1986) Spinelloid phases in the system $MgGa_2O_4$-Mg_2GeO_4. Physics and Chemistry of Minerals, 13, 382–392.

Bergerhoff, G., Hundt, R., Sievers, R., and Brown, I.D. (1983) The inorganic crystal structure database. Journal of Chemical Information and Computer Sciences, 23, 66–69.

Brown, I.D., and Altermatt, D. (1985) Bond-valence parameters obtained from a systematic analysis of the Inorganic Crystal Structure Database. Acta Crystallographica, B41, 244–247.

Canil, D. (1991) Experimental evidence for the exsolution of cratonic peridotite from high-temperature harzburgite. Earth and Planetary Science Letters, 106, 64–72.

Canil, D., O'Neill, H., and Ross, C.R., II (1990) A preliminary look at phase relations in the system Fe_3O_4-γFe_2SiO_4 at 7 GPa. Terra Abstracts, 3, 65.

Finger, L.W., Hazen, R.M., and Yagi, T. (1979) Crystal structures and electron densities of nickel and iron silicate spinels at elevated temperature or pressure. American Mineralogist, 64, 1002–1009.

Hammond, R., and Barbier, J. (1991) Spinelloids in the nickel gallosilicate system. Physics and Chemistry of Minerals, 18, 184–190.

Hazen, R.M., and Finger, L.W. (1981) Module structure variation with temperature, pressure, and composition: A key to the stability of modular structures? In A. Navrotsky and M. O'Keeffe, Eds., Structure and bonding in crystals, vol. 2, 357 p. Academic Press, New York.

——— (1982) Comparative crystal chemistry, 231 p. Wiley, New York.

Horioka, K., Takahashi, K.-I., Morimoto, N., Horiuchi, H., Akaogi, M., and Akimoto, S.-I. (1981a) Structure of nickel aluminosilicate (phase IV): A high-pressure phase related to spinel. Acta Crystallographica, B37, 635–638.

——— (1981b) Structure of nickel aluminosilicate (phase V): A high-pressure phase related to spinel. Acta Crystallographica, B37, 638–640.

Leinenweber, K., and Navrotsky, A. (1989) Thermochemistry of phases in the system $MgGa_2O_4$-Mg_2GeO_4. Physics and Chemistry of Minerals, 16, 497–502.

Ma, C.-B. (1974) New orthorhombic phases on the join $NiAl_2O_4$ (spinel analog)-Ni_2SiO_4 (olivine analog): Stability and implications to mantle mineralogy. Contributions to Mineralogy and Petrology, 45, 257–279.

Ma, C.-B., and Sahl, K. (1975) Nickel aluminosilicate, phase III. Acta Crystallographica, B31, 2142–2143.

Ma, C.-B., Sahl, K., and Tillmans, E. (1975) Nickel aluminosilicate, phase I. Acta Crystallographica, B31, 2137–2139.

Ma, C.-B., and Tillmans, E. (1975) Nickel aluminosilicate, phase II. Acta Crystallographica, B31, 2139–2141.

Price, G.D. (1983) Polytypism and the factors determining the stability of spinelloid structures. Physics and Chemistry of Minerals, 10, 77–93.

Price, G.D., Parker, S.C., and Yeomans, J. (1985) The energetics of polytypic structures: A computer simulation of magnesium silicate spinelloids. Acta Crystallographica, B41, 231–239.

Ringwood, A.E., and Major, A. (1970) The system Mg_2SiO_4-Fe_2SiO_4 at high pressures and temperatures. Physics of the Earth and Planetary Interiors, 3, 89–108.

Takahashi, E., and Ito, E. (1987) Mineralogy of mantle peridotite along a model geotherm up to 700 km depth. In M. Maghnani and Y. Syano, Eds., High pressure research in mineral physics, p. 427–438. American Geophysical Union, Washington, DC.

Manuscript received July 22, 1991
Manuscript accepted January 5, 1992